OCEAN DIGEST

Quarterly Newsletter of the Ocean Society of India

Volume 7 | Issue 4 | October 2020 | ISSN 2394-1928

Insights on the Variability of Satellite Sea Surface Salinity in the North Indian Ocean during the Southwest Monsoon of 2020



V.S.N.Murty[1], Heather L. Roman Stork[2] and Bulusu Subrahmanyam[2]
[1]CSIR-National Institute of Oceanography Regional Centre, Visakhapatnam 530 017, India
[2]School of the Earth, Ocean and Environment, University of South Carolina, Columbia, SC 29208, USA

Abstract

Analysis of Soil Moisture Active Passive (SMAP) mission processed Sea Surface Salinity (SSS) data and GPM precipitation data together with Optimum Interpolation (OI) Sea Surface Temperature (SST) data and ERA5 instantaneous surface moisture flux data in the North Indian Ocean is carried out for the southwest monsoon of 2020 (1 June-17 August). Forecasts of NEMO temperature and salinity and blended altimetry-derived surface current data are also analyzed. All the data are filtered for 3-7-day synoptic oscillations (SOs), and 10-20-day and 30-90-day intraseasonal oscillations (ISOs). The occurrence of SO peaks in moisture flux and ocean heat content in the southeastern Arabian Sea appears to set the 2020 monsoon onset on 1 June over the Kerala coast. This study reveals that the 30-90-day ISOs with larger amplitudes in SSS, SST and precipitation occur in a sequence with SSS leading SST followed by precipitation in the northern Bay and augmented (suppressed) precipitation as part of active (break) phases of the monsoon.

1. Introduction

The southwest monsoon is a dynamically complex system with oceanic processes and air-sea interactions that can significantly impact the timing of onset and total monsoon rainfall over the Indian Subcontinent. Low salinity water transported by the East India Coast Current (EICC) and North Equatorial Current (NEC) from the Bay of Bengal (BoB) and Andaman Sea into the southeastern Arabian Sea (SEAS) during boreal winter and the resulting salinity stratified upper layer in the SEAS allows the formation of a barrier layer (water column between the deep isothermal layer and shallow mixed layer) in the SEAS. This barrier layer prevents entrainment cooling and allows for establishment of the Arabian Sea Mini Warm Pool (ASMWP; Nyadjro et al., 2012; Roman-Stork et al., 2020a). The warm pool in turn allows for increased atmospheric moisture flux and the genesis of the monsoon onset vortex over the SEAS.

The 2020 southwest monsoon onset took place on the usual date of 1st June 2020 despite extremely weak EICC flow following the strong positive Indian Ocean Dipole (pIOD) in 2019 (Roman-Stork & Subrahmanyam, 2020). It is our intention to look into some insights that satellite derived Sea Surface Salinity (SSS) can be made use of in line with other satellite observational data viz., Sea Surface Temperature, Sea Surface Height, surface winds etc. in understanding the upper ocean processes and monsoon dynamics in the BoB and SEAS. In this study, we use satellite observations of SSS in concert with model forecasts in order to understand the upper ocean processes and air-sea interactions that contributed to 2020 monsoon onset in the SEAS, as well as analyze how high frequency synoptic oscillations (SOs) and intraseasonal oscillations (ISOs) in SSS impacted the BoB and monsoon precipitation over the BoB and Monsoon Core Region (MCR) of the Indian Subcontinent during the 2020 southwest monsoon.

2. Data and Methods

2.1 Data

Satellite data from the joint National Aeronautics and Space Administration (NASA)/ Japan Aerospace Exploration Agency (JAXA) Global Precipitation Measurement (GPM) mission were taken from NASA's Earthdata database (Huffman et al., 2019). The near real time (NRT) merged product combines observations from both microwave and infrared imagery from available satellites in the meteorological constellation along with GPM in daily format as a near-global 0.1° gridded product. Satellite SSS observations from NASA's Soil Moisture Active Passive (SMAP) mission processed by NASA's Jet Propulsion Lab (JPL) were obtained from NASA's PO.DAAC and are available on a daily 0.25° grid (Entekhabi et al., 2010; Fore et al., 2016). Geostrophic currents derived from blended satellite altimetric observations were obtained from Copernicus Marine (CMEMS; https://marine.copernicus.eu/) using all available altimetric observations and blended into a NRT global daily product on a 0.25° grid (Ducet et al., 2000; Le Traon et al., 1998).

Atmospheric reanalysis data on instantaneous moisture flux downloaded from the European Centre for Medium-Range Forecasting (ECMWF)'s ERA5 were used in this study. ERA5 is the successor to ERA-Interim reanalysis and is available from 1978 to present on a 0.25° grid on a single level and hourly temporal resolution (Hersbach et al., 2020). Forecasts from Nucleus for European Modeling of the Ocean (NEMO) version 3.1 are used from CMEMS and are available as daily 10-day forecasts for the past 2 years with 50 vertical layers on a 1/12° grid (Madec, 2011; Momin et al., 2013).

2.2 Methods

Time series data were bandpass filtered using a 4th order Butterworth bandpass filter and were double filtered to avoid edge effects, a methodology which has been reliably used to isolate intraseasonal oscillations and synoptic signals in the northern Indian Ocean (Krishnamurti et al., 2017; Roman-Stork et al., 2019; Roman-Stork et al., 2020c; Subrahmanyam et al., 2020).
Mixed layer depth (MLD), isothermal layer depth (MLD), and barrier layer thickness (BLT) were calculated as in Roman-Stork et al. (2020c) and Roman-Stork & Subrahmanyam (2020) using NEMOv3.1 daily model forecasts. A 0.03 kg/m^3 density criterion is used for MLD and BLT calculations, which is appropriate for tropical regions with significant diurnal variability (de Boyer Montégut et al., 2004). MLD and ILD were both calculated with a temperature difference criterion of 0.2°C. BLT is defined as the difference between ILD and MLD (BLT=ILD-MLD). Upper ocean heat content (OHC) from 0-45m layer in the SEAS was calculated as in Roman-Stork *et al.* (2020a) and Roman-Stork & Subrahmanyam (2020) using NEMOv3.1 daily model forecasts, using the equation:

$$OHC = \int_{45\ m}^{0\ m} \rho C_p T dz$$

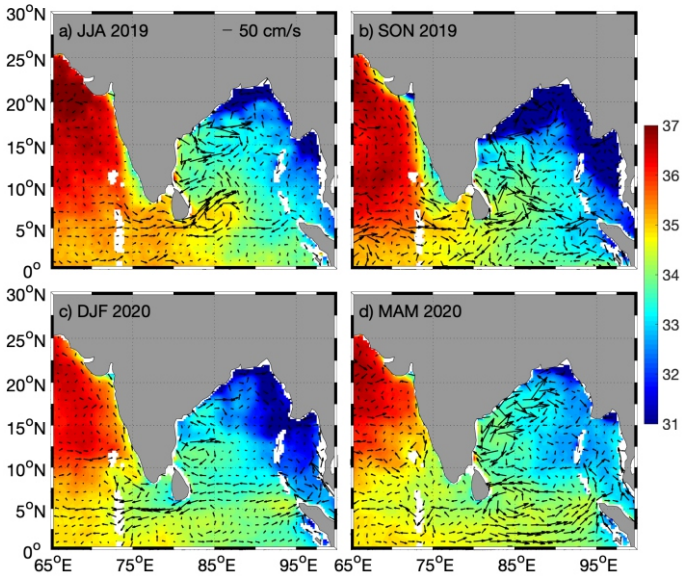

Figure 1. Seasonal averages of SMAP sea surface salinity (SSS; shaded; psu) overlaid with geostrophic currents derived from CMEMS blended altimetry (vectors; cm/s) during (a) June-August 2019, (b) September-November 2019, (c) December 2019-February 2020, and (d) March-May 2020.

where OHC is calculated from 0-45 m layer, 'ρ′ is variable seawater density (kg/m^3) calculated from the equation of state, C_p is the specific heat capacity of seawater (3930 J/(kg°C); Horii et al., 2009), and T is the mean ocean temperature over the depth thickness, dz.

3. Results and Discussion

3.1 Seasonal variation of SMAP SSS in the northern Indian Ocean

To begin our investigation, we first focus on how the pIOD in 2019 impacted the salinity exchange between the BoB and Arabian Sea, as well as features of the overall circulation in the northern Indian Ocean. Figure 1 presents the seasonal variation of SMAP SSS during 2019-2020 in the north Indian Ocean overlaid with altimetric surface currents. During the southwest monsoon of 2019 (June-August), low salinity waters were confined to the northwestern Bay and the northern Andaman Sea. Local precipitation and influx of freshwater discharge from the Ganges-Brahmaputra River system into the northern Bay and from the Irrawady River into the Gulf of Martaban, northern Andaman Sea resulted in these low salinity waters. Advection of high salinity waters from the Arabian Sea via the Summer Monsoon Current (SMC) adjacent to the Sri Lanka coast into the BoB is well apparent, and an anticyclonic eddy was generated off Sri Lanka. Vinayachandran et al.(1999) reported that the SMC flows closer to the Sri Lanka coast during the pIOD. Since the 2019 southwest monsoon also witnessed the development of pIOD in the equatorial Indian Ocean, the occurrence of SMC flowing adjacent to the Sri Lanka coast is consistent with pIOD dynamics. In the western BoB, a large anticyclonic eddy is also well developed with a poleward flow at the east coast of India between 15°N and 18°N that restricts the equatorward spread of northwestern Bay low salinity waters, such that the low salinity waters spread offshore at 18°N. From the southern Andaman Sea, westward advection of low salinity waters into the southeastern BoB is also apparent.

During the post-southwest monsoon season (September-November), with the increased river discharge and monsoonal precipitation, SSS dropped rapidly and more low salinity waters occupied the northern Bay and most of the Andaman sea. As the pIOD had also intensified by this time, the associated circulation dynamics restricted the equatorward flow of the EICC and also the equatorward spread of low salinity waters to 15°N along the east coast. The 2019 southwest monsoon (June-August) anticyclonic eddy off Sri Lanka moved northwestward with a poleward flowing current off the Sri Lanka coast.

During the northeast monsoon months (December-February), the seasonal and broad NEC is well developed in the southern Bay of Bengal and intensified south of Sri Lanka and part of its flow turned towards SEAS where it is formed an anticyclonic eddy, known as the Lakshadweep High (LH, Shankar & Shetye, 1997). The NEC, upon reaching the Sri Lanka coast, bifurcated into the southeastern coastal Bay and formed into a mesoscale anticyclonic eddy. The northward surface currents in the western BoB restricted the outward spread of low salinity waters. Low salinity waters (31-32 psu) were then confined to the northeastern Bay and the Andaman Sea. The poleward flowing West India Coastal Current (WICC) was developed along the west coast of India and the SSS is relatively diluted due to inflow of low salinity waters of the BoB via the NEC flow into the SEAS and further northward along the west coast of India.

By spring (March-May) of 2020, the NEC had shifted northward and was replaced by the broad eastward flowing current in the southern BoB. The NEC still flowed westward south of Sri Lanka and poleward into the southeastern Bay. The mesoscale anticyclonic eddy had also shifted northward towards the central east coast of India. This resulted in the poleward flowing EICC.

3.2 Evolution of oceanic parameters in the southeastern Arabian Sea and 2020 monsoon onset

Having established the primary circulation features, we next explore the oceanic processes that impacted southwest monsoon onset in 2020. Figure 2 presents the time evolution of NEMO model simulated upper ocean salinity structure (shaded region) superposed with the isotherms (black contours), ILD (white line), MLD (white dashed line) and BLT (grey line) in the SEAS from 1 January to 30 June 2020. A warm layer of temperature above 30°C developed gradually from 1 April to 10 June, coinciding with the ASMWP with the progress of occurrence of low salinity (~34.5 psu) waters deepening over a thick layer up to 40 m by 22 April 2020. The ILD, which is deep (70 m) initially in January-mid-February, gradually shoaled into the thick low salinity layer by 22 April and began deepening through 30 June.

The sigma-t criterion MLD is deep up to 30 m up to mid-January and shoaled to 20 m by 22 April, then slowly deepened through 30 June. Accordingly, the BLT became thin (5 m) from 1 April to 30 June, encompassing the developing period of the ASMWP as evidenced by the rising isotherms from 22 April from deeper depths up through 27 May. The core of the Arabian Sea High Salinity Water (ASHSW) with salinity around 36.0 – 36.5 psu lies deep in the mid-thermocline (80-120 m) from 1 January to 22 April and shoaled to a shallower depth range (70-100 m) afterwards

In association with the continuous drop in unfiltered SMAP SSS from 35.5 psu to 35.0 psu from 1 January to 13 May, BLT decreased from 40 m on 12 February to 5 m on 13 May and during this period the salinity stratified

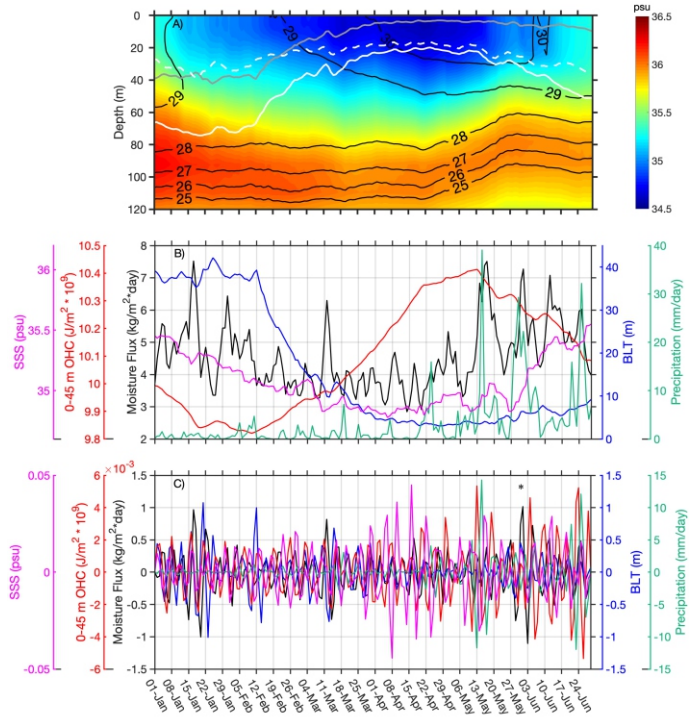

Figure 2. A) Daily NEMO salinity (shaded;psu) and temperature (black contours; C) with depth overlaid with barrier layer thickness (grey line; BLT; m), isothermal layer depth (white solid line; ILD; m), and mixed layer depth (white dashed line; MLD; m); B) unfiltered and C) 3-7-day filtered ERA5 instantaneous moisture flux magnitude (black; kg/m^{2}day), BLT (blue; m), 0-45 m layer ocean heat content (red; OHC; J/m^2 *10^9), GPM precipitation (green; mm/day), and SMAP sea surface salinity (magenta; SSS; psu) in the southeastern Arabian Sea (SEAS; 6-13N, 65-75E) during January-June 2020. The black star in (C) indicates southwest monsoon onset date, 1st June 2020

warm layer OHC increased steadily from 9.8 x 10^9 Jm^{-2} to 10.42 x 10^9 Jm^{-2}, indicating the buildup of ocean energy in the upper layer (Figure 2B). It is interesting to note that surface moisture flux and GPM precipitation reached peak higher values at the peak of OHC on 13 May. Subsequently, OHC decreased gradually from the peak value on 13 May in association with the advent of strong southwest monsoon winds brought in by the passage of the Madden-Julian Oscillation (MJO; Roman-Stork & Subrahmanyam, 2020), and during this period both the moisture flux and precipitation reached secondary peaks around 1 June. The 3-7- day filtered time series of these oceanic parameters from 1 January to 30 June exhibit large amplitude peaks (Figure 2C). During the southwest monsoon advancement over the SEAS (13 May-30 June) large amplitude peaks occurred in surface moisture flux, SSS and OHC at least partially influenced by the passage of the MJO (Roman-Stork & Subrahmanyam, 2020); however, on the day of monsoon onset over the Kerala coast, 1 June, the normal climatological monsoon onset date, surface moisture flux increased. Following the monsoon onset, the other parameters once again attained higher amplitudes, except moisture flux and BLT. The peak amplitudes of SO in OHC followed higher amplitude SO in precipitation and SSS and a weaker SO amplitude in BLT (eg. 13-15 May and 24-26 June). It is the large amplitude SO in OHC and precipitation followed by higher amplitude in surface moisture flux over the SEAS that impact monsoon rainfall and its strength. In other words, the SEAS responds to 3-7-day SO in wind speed, moisture flux and precipitation and the salinity stratified warmer upper ocean provides necessary heat energy to the overlying atmosphere.

Prior to monsoon onset, a weather disturbance NISARGA developed as monsoon onset vortex over the East Central Arabian Sea (IMD, 2020) and SEAS and it caused observed heavy precipitation in the eastern Arabian Sea during 31 May-3 June and cyclonic winds with westerly to southwesterly surface winds prevailed over the SEAS (Figure 3a) and southwesterly winds prevailed over the entire BoB. On the subsequent days, the NISARGA weakened over the MCR (see box in Figure 3a over the Indian Subcontinent) and caused precipitation there. Anticyclonic circulations are seen in the SEAS and also in the northwestern Bay. A cyclonic eddy, known as Sri Lanka Dome (SLD) (Burns*et al.*, 2017), developed northeast of Sri Lanka, along with an anticyclonic eddy off southeastern Sri Lanka. The Andaman Sea, Northern Bay and west of Andaman Islands regions experienced low salinity waters by 31 May 2020 under the influence of the first local monsoonal precipitation over the Bay. On 1 June one can notice monsoon precipitation over Kerala coast in association with the monsoon onset, and the conditions continued on 2 June (Figures 3 c,e). The surface currents and SSS in the BoB and Arabian Sea did not change appreciably between 31 May and 2 June.

3.3 The regional salinity response in the Bay of Bengal to monsoon and ISO forcing

We next examine regional variability in GPM precipitation and SMAP SSS over the BoB during the southwest monsoon of 2020 (1 June-17 August). For this, we considered three boxes one in the northern Bay (15-20N, 85-95E), central Bay (10-15N, 85-95E), and southern Bay (5-10N, 85-95E). During this period, the unfiltered or observed GPM precipitation was always high in the northern Bay compared to the central and southern Bay boxes. In the northern Bay, higher precipitation (35-70mm/day) occurred during 3-24 August (Figure not shown) in association with the synoptic weather disturbance.

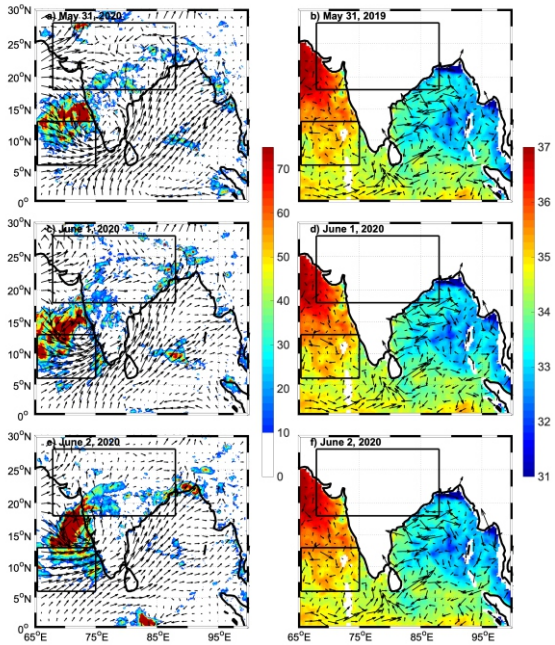

Figure 3. (a,c,e) GPM precipitation (shaded; mm/day) overlaid with CCMPv2 surface winds (black vectors; m/s) and (b,d,f) SMAP SSS (shaded; psu) overlaid with geostrophic currents derived from CMEMS blended altimetry (black vectors; cm/s) for (a-b) May 31, (c-d) June 1, and (e-f) June 2, 2020. Black boxes indicate the location of the SEAS.

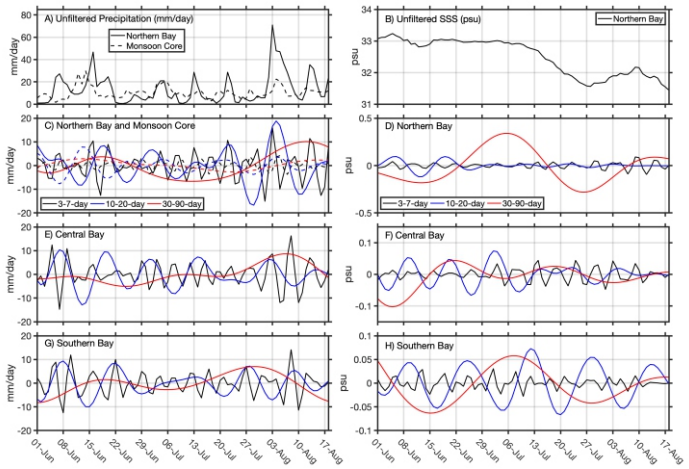

Figure 4. Unfiltered GPM precipitation (left; mm/day) and SMAP SSS (right; psu) in the (A-B) northern Bay (black solid line; 15-20N, 85-95E) and monsoon core region (in A: black dashed line; 18-28N, 78-88E) and 3-7-day filtered (black), 10-20-day (blue), and 30-90-day (red) filtered precipitation and SSS in the (C-D) northern Bay (solid lines; 15-20N, 85-95E and dashed lines; Monsoon Core region), (E-F) central Bay (10-15N, 85-95E), and (G-H) southern Bay (5-10N, 85-95E).

On 21 September, higher precipitation occurred both in the northern and central Bay boxes. On 5 occasions, higher precipitation occurred in the southern Bay box. During the observational period (1 June – 17 August), SMAP SSS is high and uniform (33.8-34.0 psu) in the southern Bay and is around 33.05 psu in the central Bay, and in the northern Bay box, SSS exhibits larger variation (33.05 psu to 31 psu) from 6 July to 17 August (Figure not shown). This large drop is partly due to local monsoonal precipitation and horizontal advection of freshwater discharge from the Ganges-Brahmaputra River system.

Figure 4A compares the observed precipitation over the northern Bay and Monsoon Core Region (MCR). Higher precipitation on 11 June over MCR is associated with the westward movement of low pressure and associated cyclonic circulations that caused widespread heavy rainfall(IMD, 2020). Subsequently, the peaks in precipitation over the MCR either coincide or lagged with peaks over the northern Bay (Figure 4A). SMAP SSS in the northern Bay exhibits larger drop (33.05 psu to 31 psu) from 6 July to 17 August (Figure 4B). GPM precipitation and SSS in each box were filtered for 3-7-day SO and 10-20-day and 30-90-day ISO (Figures 4C-H). The peaks in the observed precipitation in the northern box are due to the dominant SO peaks in precipitation. On three occasions, the 10-20-day ISO also contributed to the observed precipitation. On one event of higher precipitation (1-11 August), both the SO and ISOs contributed. The amplitudes of the SO and 10-20-day ISO in SSS are weak, but the 30-90-day ISO (the MJO) provides larger SSS variation. This 30-90-day ISO in SSS is out of phase with the 30-90-day ISO in precipitation, with a lead of one week; when 30-90-day precipitation is in its negative phase, correspondingly 30-90-day SSS shows a large positive phase, and *vice versa*. This SSS variation explains the influence of horizontal advection of relatively high salinity waters into the northern Bay box. This also shows that convection leading to precipitation is suppressed when high salinity waters prevailed over the northern Bay and higher precipitation takes place over low salinity waters. Neither the SO nor 10-20-day ISO in precipitation affected the SSS in this manner.

The convective phase of the 30-90-day ISO reached its peak value on 29 July over southern Bay, on 6 August over central Bay

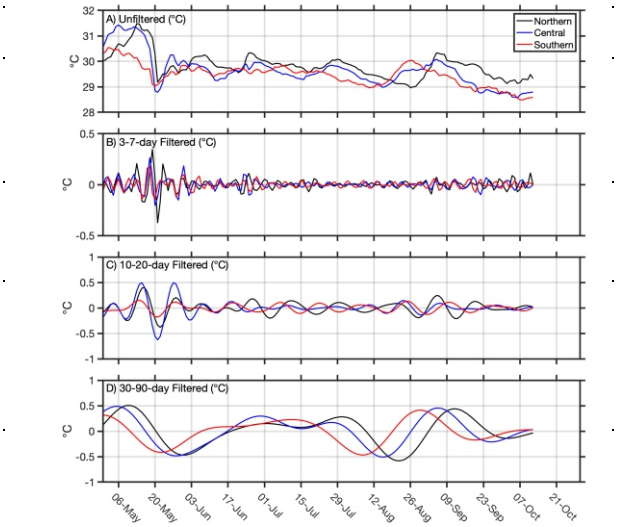

Figure 5. OISST (°C) in the northern (black; 15-20N, 85-95E), central (blue; 10-15N, 85-95E), and southern (red; 5-10N, 85-95E) Bay of Bengal that is (A) unfiltered, (B) 3-7-day filtered, (C) 10-20-day filtered, and (D) 30-90-day filtered

and on 14 August over northern Bay and this indicates the northward propagation this ISO (5° distance in 8 days) with a speed of 0.63°/day, which is in close agreement with that estimated (0.74°/day) for the propagation of 30-90-day ISO rainfall band over the BoB (Nirupam and Misra, 2020). In the central Bay and southern Bay, the 30-90-day ISO in precipitation and SSS are out of phase and of weaker amplitudes (Figure 4E-F and Figure 4G-H). In the northern Bay, the 30-90-day ISO in precipitation and SSS are too out of phase but of higher amplitudes. Here, this ISO SSS leads the ISO precipitation by 1-2 week days during 29 June – 17 August, and while the peak positive SSS occurs on 6 July, the peak negative precipitation occurs on 13 July (Figure 4C-D).Similarly, the peak negative 30-90-day ISO SSS on 26 July leads by around 2 weeks to that of peak positive precipitation on 10 August. It appears that the positive (negative) 30-90-day SSS phase during 22 June-10 August in the northern Bay is affected by the lateral movement of freshwater plume from (into) the box by surface currents and horizontal advection processes.

The 30-90-day SST amplitudes are large (±0.5°C) during 1 May-10 October in the southern, central and northern Bay (Figure 5D), while the 10-20-day SST amplitudes are large (±0.5°C) only during 15-26 May over the central Bay when the southwest monsoon winds and rains were first set over Andaman Islands (Figure 5C).The 3-7-day SST amplitude is up to ±0.3°C around 20 May in the northern Bay due to the passage of Severe Cyclonic Storm AMPHAN (Roman-Stork & Subrahmanyam, 2020)over the northern BoB (Figure 5B). From 20 May to 10 October, the amplitudes of 3-7-day and 10-20-day SST are weak, as the unfiltered SST varied over a narrow range, 29.2°-30.2°C (Figure 5A). The 30-90-day ISO in SST propagated northward and the MJO cooling (negative SST) phase speed decreased from 1°/day from southern to central Bay to 0.56°/day from central to northern Bay. The MJO warming (positive SST) phase speed increased from 0.62°/day from southern to central Bay to 1°/day from central Bay to northern Bay, with a mean MJO period of 42 days (Figure 5D). The MJO SST cooling phase is associated with the active phase of MJO precipitation over the northern Bay, and MJO SST warming phase with the

suppressed convection (negative precipitation phase) or break phase of MJO. As the transition takes place from the break phase (suppressed convection) to the active phase (enhanced convection), first lower SSS waters (31.6 psu) prevailed on 27 July (due to horizontal advection of river discharge waters or freshwater plume into the box) with a peak negative MJO SSS (-0.3 psu) and this was followed by warmer MJO SST (0.3°C) with a lag of 2-4 days (29-31 July) and an active phase of maximum MJO precipitation peaks after about 2 weeks, around 10 August. The active phase MJO SST reaches peak negative value on 23 August (Figure 5D). Thus, it is seen that in the northern Bay, the lateral movement of freshwater plume of river discharge waters into the box and away from the box under the influence of surface currents and horizontal advection processes plays an important role to set the 30-90-day ISO SSS phase which further sets the SST phase and this influences the convection phase leading either to suppressed convection or enhanced precipitation as part of break or active phases of MJO precipitation during the southwest monsoon. Thus, the above information provides new insights on the use of satellite SSS variability along with the other satellite data products to study the southwest monsoon and its impact and dynamics in the southeastern Arabian Sea and Bay of Bengal.

4. Conclusions

The 2020 southwest monsoon season was heavily impacted by the 2019 pIOD, ISO and SO processes, and tropical system of Cyclone Amphan in May 2020. While the EICC was significantly weakened by the pIOD, the NEC was persistent and strong, allowing for sufficient freshwater to enter the SEAS. Additional moisture flux was added to the SEAS by the MJO and Cyclone Amphan and SO in moisture flux reached peak on 1 June, when the monsoon onset took place over Kerala coast. The stratified, warmer upper ocean in the SEAS provides the heat energy necessary to the overlying atmosphere such that it responds to 3-7-day SO in SSS, moisture flux, OHC, surface winds, and precipitation around monsoon onset. The ISOs were also important for monsoon precipitation, with the northward propagating convective phase of MJO providing a strong background signal in the BoB and impacted the upper ocean in the BoB. Satellite SSS is found to be a useful parameter in the monsoon dynamics studies and its 30-90-day ISO SSS variability has a large amplitude in the northern Bay and it leads the 30-90-day ISO SST by a few days, which then impacted the 30-90-day ISO precipitation to reach a peak after a week days over the northern Bay and these combinations in a sequence contributed to the active and break phases of the southwest monsoon 2020.

Acknowledgements

The lead author acknowledges the Ministry of Earth Sciences (MoES), New Delhi for the Ocean Mixing and Monsoons Project under the National Monsoon Mission, and is thankful to the Director General CSIR and Director, CSIR-NIO for the financial grant of CSIR-Emeritus Scheme and for the Scientist-in-Charge, CSIR-NIO RC Visakhapatnam for their keen interest. The authors BS and Roman-Stork got this research support through the United States Office of Naval Research's Oceanic Control of Monsoon Intra-seasonal Oscillations in the Tropical Indian Ocean and the Bay of Bengal (MISO-BOB) Award# N00014-17-1-2468 awarded to BS. The SMAP-CAP V4.3 data used are produced by NASA's Jet Propulsion Lab, Pasadena, CA and are available through PO.DAAC (https://podaac-tools.jpl.nasa.gov/drive/files/SalinityDensity/smap/L3_/JPL/V4.3/8day_running). ECMWF ERA5 atmospheric data are available at https://cds.climate.copernicus.eu/cdsapp#!/dataset/reanalysis-era5-single-levels?tab=overview. NOAA OISST v2 is obtained from NOAA's Physical Sciences Laboratory (PSL) at https://psl.noaa.gov/data/gridded/data.noaa.oisst.v2.highres.html. Data from NASA/JAXA's GPM's NRT merged product were obtained from NASA's Earthdata database at daily temporal resolution (https://pmm.nasa.gov/data-access/downloads/gpm). NRT CCMPv2.0 winds were obtained from RSS athttp://www.remss.com/measurements/ccmp/. CMEMS NRT blended daily geostrophic currents were obtained from https://resources.marine.copernicus.eu/?option=com_csw&view=details&product_id=SEALEVEL_GLO_PHY_L4_NRT_OBSERVATIONS_008_046. NEMOv3.1 model simulations are available from CMEMS in a two-year moving window (http://marine.copernicus.eu/services-portfolio/access-to-products/?option=com_csw&view=details&product_id=GLOBAL_ANALYSIS_FORECAST_PHY_001_024).

References:

Burns, J.M., Subrahmanyam, B., Murty, V.S.N.(2017). On the dynamics of the Sri Lanka dome. Journal of Geophysical Research:Oceans, 122, 7737–7750. https://doi.org/10.1002/2017JC012986.

de Boyer Montégut, C., Madec, G., Fischer, A. S., Lazar, A., & Iudicone, D. (2004). Mixed layer depth over the global ocean: An examination of profile data and a profile-based climatology. Journal of Geophysical Research C: Oceans, 109(12), 1–20. https://doi.org/10.1029/2004JC002378

Ducet, N., Le Traon, P. Y., & Reverdin, G. (2000). Global high-resolution mapping of ocean circulation from TOPEX/Poseidon and ERS-1 and -2. Journal of Geophysical Research: Oceans, 105(C8), 19477–19498. https://doi.org/10.1029/2000jc900063

Entekhabi, D., Njoku, E. G., O'Neill, P. E., Kellogg, K. H., Crow, W. T., Edelstein, W. N., et al. (2010). The soil moisture active passive (SMAP) mission. Proceedings of the IEEE, 98(5), 704–716. https://doi.org/10.1109/JPROC.2010.2043918

Fore, A. G., Yueh, S. H., Tang, W., Stiles, B. W., & Hayashi, A. K. (2016). Combined Active/Passive Retrievals of Ocean Vector Wind and Sea Surface Salinity With SMAP. IEEE Transactions on Geoscience and Remote Sensing, 54(12), 7396–7404. https://doi.org/10.1109/TGRS.2016.2601486

Hersbach, H., Bell, B., Berrisford, P., Hirahara, S., Horányi, A., Muñoz-Sabater, J., et al. (2020). The ERA5 global reanalysis. Quarterly Journal of the Royal Meteorological Society, 146(730), 1–51. https://doi.org/10.1002/qj.3803

Horii, T., Masumoto, Y., Ueki, I., Hase, H., & Mizuno, K. (2009). Mixed layer temperature balance in the eastern Indian Ocean during the 2006 Indian Ocean dipole. Journal of Geophysical Research: Oceans, 114(7), 1–14. https://doi.org/10.1029/2008JC005180

Huffman, G. J., Bolvin, D. T., Braithwaite, D., Hsu, K.-L., Joyce, R. J., Kidd, C., et al. (2019). Integrated Multi-satellite Retrievals for the Global Precipitation Measurement (GPM) Mission (IMERG), (March), 343–353. https://doi.org/10.1007/978-3-030-24568-9_19

IMD (2020). Southwest Monsoon 2020: All India Monthly Weather Report for June 2020 prepared by India Meteorological Department, ESSO, Ministry of Earth Sciences, Government of India, 14 pp. http://mausam.imd.gov.in.

Krishnamurti, T. N., Jana, S., Krishnamurti, R., Kumar, V., Deepa, R., Papa, F., et al. (2017). Monsoonal intraseasonal oscillations in the ocean heat content over the surface layers of the Bay of Bengal. Journal of Marine Systems, 167, 19–32. https://doi.org/10.1016/j.jmarsys.2016.11.002

Madec, G. (2011). NEMO Ocean Engine: version 3.3, (27), 1–332.

Retrieved from http://www.nemo-ocean.eu/About-NEMO/Referencemanuals%5Cnpapers2://publication/uuid/73E7FF17-99BE-4B10-A823-0037C823EF6E
Momin, I. M., Mitra, A. K., Mahapatra, D. K., Rajagopal, E. N., & Harenduprakash, L. (2013). Indian Ocean simulation results from NEMO global ocean model. *Indian Journal of Marine Sciences*, *42*, 425–430.
Nirupam, K. & V. Misra (2020). Differences in northward propagation of convection over the Arabian Sea and Bay of Bengal during boreal summer, Journal of Geophysical Research – Atmosphere, 125 (3), https://doi.org/10.1029/2019JD031648.
Nyadjro, E. S., Subrahmanyam, B., Murty, V. S. N. & Shriver, J. F. (2012). The role of salinity on the dynamics of the Arabian Sea Mini Warm Pool. *J. Geophys. Res. Ocean.***117**, 1–12.
Roman-Stork, H. L., Subrahmanyam, B., & Murty, V. S. N. (2019). Quasi-biweekly oscillations in the Bay of Bengal in observations and model simulations. *Deep-Sea Research Part II: Topical Studies in Oceanography*, *168*(June), 104609. https://doi.org/10.1016/j.dsr2.2019.06.017
Roman-Stork, H. L., Subrahmanyam, B., & Murty, V. S. N. (2020a). The Role of Salinity in the Southeastern Arabian Sea in Determining Monsoon Onset and Strength. *Journal of Geophysical Research: Oceans*, *125*(1). https://doi.org/10.1029/2019jc015592
Roman-Stork, H. L., Subrahmanyam, B., & Murty, V. S. N. (2020b). Role of 3-7-day synoptic oscillations on southwest monsoon onset and rainfall over India. *Scientific Reports* (under revision)
Roman-Stork, H. L., Subrahmanyam, B., & Trott, C. B. (2020c). Monitoring Intraseasonal Oscillations in the Indian Ocean Using Satellite Observations. *Journal of Geophysical Research: Oceans*, *125*(2), 1–22. https://doi.org/10.1029/2019jc015891
Roman-Stork, H. L., & Subrahmanyam, B. (2020). The Impact of the Madden–Julian Oscillation on Cyclone Amphan (2020) and Southwest Monsoon Onset. *Remote Sensing*, *12*(18), 3011. https://doi.org/10.3390/rs12183011
Shankar, D. & S.R. Shetye (1997). On the dynamics of the Lakshadweep high and low in the southeastern Arabian Sea. *J. Geophysical Research – Oceans*, **https://doi.org/10.1029/97JC00465**
Subrahmanyam, B., Roman-Stork, H. L., & Murty, V. S. N. (2020). Response of the Bay of Bengal to 3-7-day synoptic oscillations during the southwest monsoon of 2019. *Journal of Geophysical Research : Oceans*, *125*, 1–28. https://doi.org/10.1029/2020JC016200
Le Traon, P. Y., Nadal, F., & Ducet, N. (1998). An improved mapping method of multisatellite altimeter data. *Journal of Atmospheric and Oceanic Technology*, *15*(2), 522–534. https://doi.org/10.1175/1520-0426(1998)015<0522:AIMMOM>2.0.CO;2
Vinayachandran, P. N., Y. Masumoto, T. Mikawa, & T. Yamagata (1999). Intrusion of the Southwest Monsoon Current into the Bay of Bengal,*Journal of Geophysical Research-Oceans*, **104**, 11,077-11,085.

Environmental Magnetism and its Application in Gas Hydrate Studies

Dr. Firoz Badesab
Scientist
Geological Oceanography Division
CSIR-National Institute of Oceanography
Dona Paula-403004, Goa
Email: firoz@nio.org

Magnetic minerals are ubiquitous and important sediment constituents in coastal and marine sedimentary system. Number of environmental processes alters the primary magnetic mineral assemblages by imprinting changes in the magnetic mineral content, grain size and mineralogy which can be easily detected using magnetic techniques (Evans & Heller, 2003). Major factors which can significantly modify the environmental magnetic properties includes sediment source, climatic changes, weathering and erosion, transport conditions, depositional environment, diagenesis, authigenic, biogenic and anthropogenic processes (Roberts, 2015). Hence, magnetic minerals have been extensively utilized as potential markers for resolving range of geological problems (Oldfield et al., 1985; Thompson & Oldfield, 1986). Application of environmental magnetic techniques in context with gas hydrate research is presented.

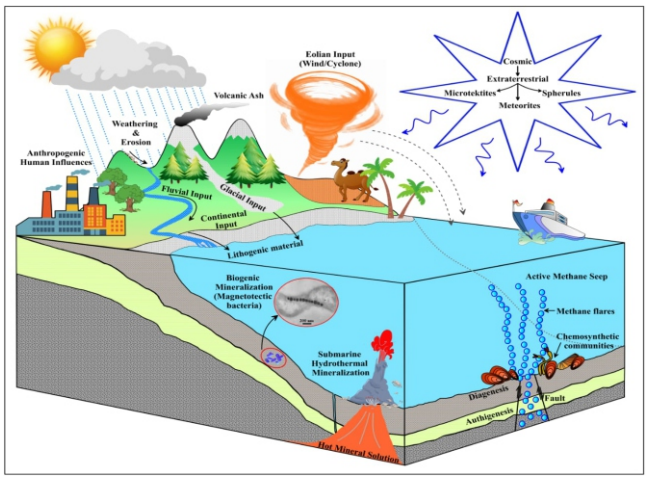

Figure 1. Schematic illustration explaining potential sources of magnetic minerals in coastal and marine sedimentary system (Modified from *Friederich et al., 1999*).

Magnetic Exploration of Gas Hydrates in the Bay of Bengal

Methane hydrate is the most common and natural form of gas hydrates, and is distributed worldwide along the oceanic and permafrost environments (Kvenvolden, 1993). In methanic sediment, geochemical processes linked with the formation and dissociation of methane results in the formation of new (secondary – diagenetic/authigenic) minerals which has can be easily tracked using magnetic methods (Housen and Musgrave, 1996; Dewangan et al., 2013). During the first national gas hydrate expedition (NGHP-EXP-01) onboard D/V JOIDES Resolution, gas hydrates were discovered from several locations in the Krishna-Godavari (K-G) basin, Bay of Bengal (Kumar et al., 2014). Rock magnetic studies were conducted on the sediment cores retrieved from these locations to accomplish (a) establish the linkage between gas hydrates and associated magnetic signals, (b) fingerprinting complex magnetic mineralogical signatures formed as a result of gas hydrate related processes, and (c) unravel the mechanism of formation and preservation of iron sulfides in gas hydrate bearing sediments. Below are some of the research highlights:

The study by Badesab et al. (2017, 2019a) unravelled the linkages between sedimentation, shale tectonics, magnetite enrichment, diagenesis, and gas hydrate formation in the Krishna-Godavari basin. They identified

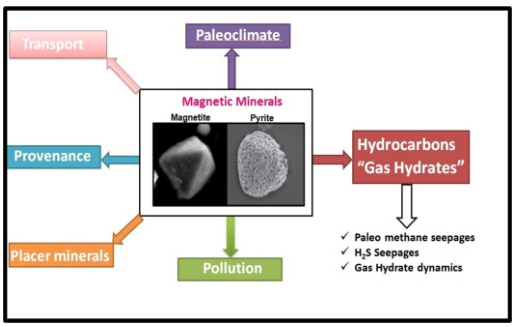

Figure 2. Schematic illustration highlighting applications of environ and rock magnetism

an anomalous band of elevated magnetite content formed as a result of high-sedimentation events in the K-G basin. A well-developed fault system that provided conduits for upward methane migration and supported hydrate formation. Diagenetically formed iron sulfides were found to occur within the magnetite-rich band suggesting that fault system favoured their growth by facilitating episodic methane supply from deeper sources. A magnetic based proxy has been developed to constrain paleo-methane seepage events in marine sediments. The study highlighted that the magnetic mineralogical approach has wider scope to constrain the understanding of gas hydrate systems in marine sediments

A dedicated study by Badesab et al., 2019bconducted specialized rock-magnetic and transmission electron microscope (TEM) analyses on the samples from a sediment core and constrain the formation and preservation of greigite in shallow sediments and how this might link to reactions involving methane. Following are the key highlights of this work.(a) Delineated the controls on greigite production and preservation in a gas hydrate system of the Krishna-Godavari basin, Bay of Bengal. (b) Reported the occurrence of silicate-hosted greigite inclusion in gas hydrate system for the first time

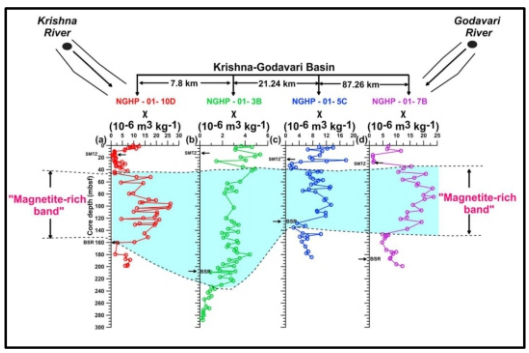

Figure 3. Magnetic susceptibility records of sediment cores retrieved from potential gas hydrate sites in the Krishna-Godavari (K-G) basin, Bay of Bengal. An anomalous magnetite rich band showing increased magnetic susceptibility is highlighted by a blue color (Modified from Badesab et al., 2019a).

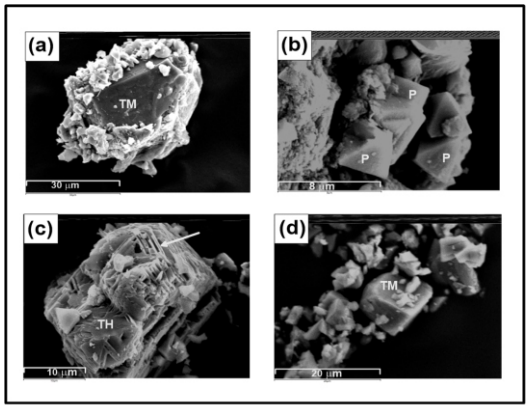

Figure 4. Detrital and diagenetically formed iron oxides and sulfides (a, c, d): Detrital coarse grained titanomagnetite & titanohematite, (b): Diagenetic pyrite

Rockmagnetic identification of Greigite – FORC Diagrams

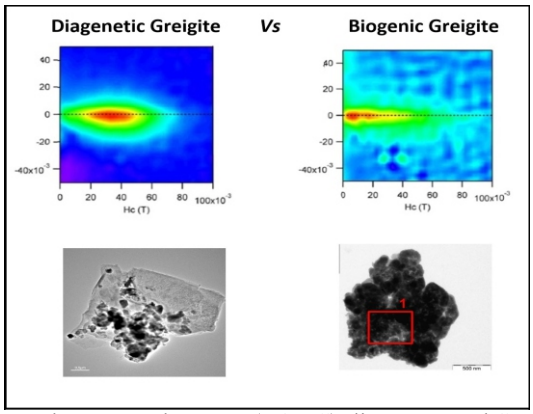

Figure 5. First-order reversal curves (FORC) diagrams and SEM images discriminating the diagenetic and biogenic greigite identified in the sediment core from gas hydrate proven site in the K-G basin.

References:

Badesab, F., Dewangan, P., Usapkar, A., Kocherla, M., Peketi, A., Mohite, K., et al. (2017). Controls on evolution of gas-hydrate system in the Krishna-Godavari basin, offshore India. *Geochemistry, Geophysics, Geosystems,* 18(1), 52–74. https://doi.org/10.1002/2016GC006606

Badesab, F., Dewangan, P., Gaikwad, V., Kars, M., Kocherla, M., Krishna, K.S., et al. (2019a). Magnetic mineralogical approach for exploration of gas hydrates in the Bay of Bengal. *Journal of Geophysical Research: Solid Earth,* 24(5), 4428–4451.https://doi.org/10.1029/2019JB017466

Badesab, F., Gaikwad, V., & Dewangan, P. (2019b). Controls on greigite preservation in a gas hydrate system of the Krishna-Godavari basin, Bay of Bengal. *Geo-Marine Letters,* 40(4), 439-452. https://doi.org/10.1007/s00367-019-00604-z

Dewangan, P., N. Basavaiah, F. K. Badesab, A. Usapkar, A. Mazumdar, R. Joshi, and T. Ramprasad (2013), Diagenesis of magnetic minerals in a gas hydrate/cold seep environment off the Krishna–Godavari basin, Bay of Bengal, Mar. Geo., 340, 57–70.

Evans, M. E., and F. Heller (2003), Environmental Magnetism: Principles and Applications of Enviromagnetism, 86. Int. Geophys. Ser., 293 pp.,Academic, New York.

Housen, B. A., and R. J. Musgrave (1996), Rock-magnetic signature of gas hydrates in accretionary prism sediments, Earth Planet. Sci. Lett., 139(3–4), 509–519.

Kumar P., et al. (2014), the NGHP Expedition 01 Scientific Party Geologic implications of gas hydrates in the offshore of India: Krishna– Godavari basin, Mahanadi basin, Andaman Sea, Kerala–Konkan basin, Mar. Pet. Geol., 58, Part A, 3–28.

Kvenvolden, K. (1993), Gas hydrates-geological perspective and global change, Rev Geophys., 31, 173–187, doi:10.1029/93RG00268.

Oldfield, F., Maher, B. A., Donoghue, J., & Pierce, J. (1985). Particle-size related, mineral magnetic source sediment linkages in the Rhode River catchment, Maryland, USA. *Journal of the Geological Society, 142,* 1035–1046. https://doi.org/10.1144/gsjgs.142.6.1035

Roberts, A. P. (2015). Magnetic mineral diagenesis. *Earth-Science Reviews, 151,* 1–47. https://doi.org/10.1016/j.earscirev.2015.09.010

Thompson, R., and F. Oldfield (1986), Environmental Magnetism, 227 pp., Allen and Unwin, London.

Living benthic foraminifera from the Bay of Bengal oxygen minimum zone

Thejasino Suokhrie
Micropaleontology Lab,
CSIR-National Institute of Oceanography,
Dona Paula, Goa
tsuokhrie@nio.org

In a warming world, depletion of oxygen from oceans poses a major threat. There are zones in the ocean where the utilization of dissolved oxygen increases tremendously with little replenishment giving rise to dead zones or Oxygen Minimum Zones (OMZ). The expanding OMZs are a cause of major concern as they are the source for production of N_2O by processes like denitrification of which the Arabian Sea is a major contributor (Naqvi et al., 2000; Stramma et al., 2005; Bange et al., 2005). Interestingly, at the same latitude in the Bay of Bengal, despite of the presence of OMZ reportedly within ~100-1000 m depth, denitrification is not observed for various reasons (Rao et al., 1994; Sarma, 2002; Bristow et al., 2017). This marked difference in OMZ between the Arabian Sea and Bay of Bengal could support different benthic fauna. The benthic fauna of particular interest are calcareous microfossils called 'foraminifera'. Foraminifera are eukaryotic microorganisms, ubiquitous in marine sediments and extremely reliable as a tool to decipher environmental/climatic changes in the past as its hard shell preserves even the slightest of change in its ambient environment (Murray et al., 2006). Unlike Arabian Sea, documentation of living benthic foraminifera from OMZ of Bay of Bengal is limited. Such a knowledge will enhance our understanding of the intensity of OMZ from these two regions.

The sediments samples from a water depth of ~27 m to ~2494 m were collected from the west-central Bay of Bengal covering the region between major rivers, namely Krishna-Godavari, Pennar and Cauvery, by using a 'multi-corer'. The top 0-2 cm of the sediment sample were processed at the Micropaleontology Laboratory, CSIR-National Institute of Oceanography, Goa. Benthic foraminifera were separated from the sediment and species were identified. The dissolved oxygen concentration was found to be significantly low at the depths between ~100 m to ~1000 m, having average value of ~0.5 ml/l. Hence the abundance of benthic species within these depths were segregated. Overall, benthic foraminiferal abundance at these depths was high but less diverse, suggesting stressed environment at 100-1000 m. Only a few stress tolerant species were highly abundant and made up for the total population. A total of 20 species were found to have a statistically significant correlation with low dissolved oxygen in the bay. A comparison with earlier reports from the Arabian Sea show that only 4 species were common in both the regions. Hence, 16 species specific to the Bay of Bengal OMZ were identified and can be utilised as indicator species (Suokhrie et al., 2020).

Previous reports suggest the presence of denitrification activity in foraminifera wherein they store and create a nitrate pool intracellularly and utilise it for complete denitrification. The ability of these microorganism to respire nitrate rather than oxygen has been described as rare amongst eukaryotes and to the extent that this respiration pathway is sometimes preferred even in the presence of oxygen (Glock et al., 2019). Some of the denitrifying benthic foraminiferal species were reported earlier from the Arabian Sea OMZ. But, none of these species were recorded from the Bay of Bengal OMZ. This indicates that the marked difference in species between these two regions is likely due to the absence of active denitrification in Bay of Bengal OMZ. Bay of Bengal is suggested to be on a tipping point to become an active site for anoxia and denitrification. The fact that foraminiferal population is highly abundant (~5000 individuals/g sediment) in the OMZ, combined with the ability of denitrification by a few of these species, suggests that there is a scope of exploring the contribution of benthic foraminifera to the nitrogen fixing processes in the Bay of Bengal, in future.

Acknowledgements

This work is part of the PhD work done by the author at CSIR-NIO. Director, CSIR-NIO is acknowledged for permission to carry out the work. TS is grateful to Dr. Rajiv Nigam and Dr. Rajeev Saraswat, CSIR-NIO, for their continuous support.

References:

Bange, H. W., Naqvi, S. W. A., Codispoti, L. A., 2005. The nitrogen cycle in the Arabian Sea. *Progress in Oceanography*, 65, 145-158.

Bristow, L. A., Callbeck, C. M., Larsen, M., Altabet, M. A., Dekaezemacker, J., Forth, M., Gauns, M., Glud, R. N., Kuypers, M. M., Lavik, G. Milucka, J., 2017. N_2production rates limited by nitrite availability in the Bay of Bengal oxygen minimum zone. *Nature Geoscience*, 10, 24-29.

Glock, N., Roy, A. S., Romero, D., Wein, T., Weissenbach, J., Revsbech, N. P., Høgslund, S., Clemens, D., Sommer, S., Dagan, T., 2019. Metabolic preference of nitrate over oxygen as an electron acceptor in foraminifera from the Peruvian oxygen minimum zone. *Proceedings of the National Academy of Sciences*, 116, 2860-2865.

Murray, J. W., 2006. Ecology and applications of benthic foraminifera. Cambridge University Press.

Naqvi, S. W. A., Jayakumar, D. A., Narvekar, P. V., Naik, H., Sarma, V. V. S. S., D'souza, W., Joseph, S., George, M. D., 2000. Increased marine production of N_2O due to intensifying anoxia on the Indian continental shelf. *Nature*, 408, 346-349.

Rao, C. K., Naqvi, S.W.A., Kumar, M. D., Varaprasad, S. J. D., Jayakumar, D. A., George, M.D., Singbal, S.Y.S., 1994. Hydrochemistry of the Bay of Bengal: possible reasons for a different water-column cycling of carbon and nitrogen from the Arabian Sea. *Marine Chemistry*, 47, 279-290.

Suokhrie, T., Saraswat, R., Nigam, R., 2020. Lack of denitrification causes a difference in benthic foraminifera living in the oxygen deficient zones of the Bay of Bengal and the Arabian Sea. *Marine Pollution Bulletin*, 153, 110992.

Stramma, L., Prince, E. D., Schmidtko, S., Luo, J., Hoolihan, J. P., Visbeck, M., Wallace, D. W., Brandt, P., Körtzinger, A., 2012. Expansion of oxygen minimum zones may reduce available habitat for tropical pelagic fishes. *Nature Climate Change*, 2, 33-37.

Sarma, V.V.S.S., 2002. An evaluation of physical and biogeochemical processes regulating the oxygen minimum zone in the water column of the Bay of Bengal. *Global biogeochemical cycles*, 16, 46-1.

Research Highlights

The IOD impacts on Indian Ocean Carbon Cycle



Vinu Valsala, Scientist F, IITM (MoES), Pune
Sreeush M. G., Postdoc, IBS, Korea
Kunal Chakraborty, Scientist E, INCOIS (MoES), Hyderabad

Based on the following paper:
Valsala, V., Sreeush, M. G., & Chakraborty, K. (2020). The IOD impacts on the Indian Ocean carbon cycle. *Journal of Geophysical Research: Oceans*, 125, e2020JC016485. https://doi.org/10.1029/2020JC016485

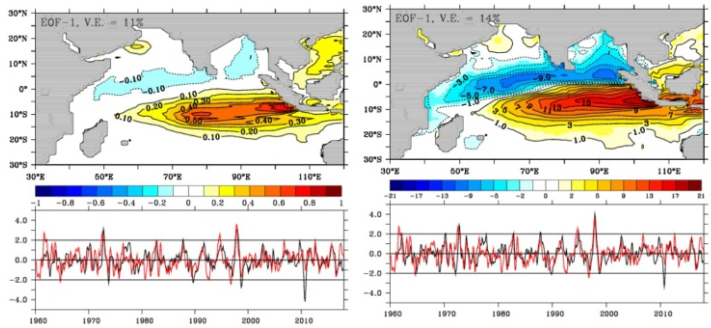

Figure 1. (left) EOF-1 loading of surface ocean sea-to-air CO_2 flux anomalies (mole m^{-2} yr^{-1}) from 1960-2019 and corresponding principle component (PC-1; black color) and normalized dipole mode index (DMI), as in Saji et al. (1999) (red line). (right) The corresponding EOF-1 of the surface ocean pCO_2 anomalies (µatm). The correlation coefficient between PC-1 and DMI is above 0.4 which is above the 99% significance level.

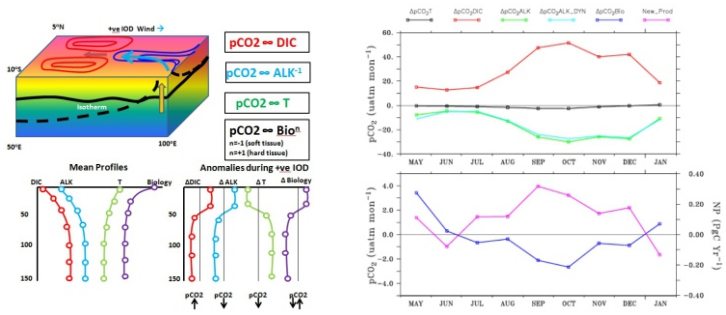

Figure 2. (left) The mechanism of IOD and Indian Ocean Carbon Cycle variability. During positive IOD, the upwelling and *nutricline* shoaling in the southeastern tropical Indian Ocean brings carbon, alkalinity & nutrient rich water to the surface. Surface ocean pCO_2 increases with increase in carbon rich water and decreases with alkalinity rich water. On the other hand pCO_2 decreases with cold upwelling. Biological impact on pCO_2 is a decrease in pCO_2 with the increase in soft-tissue pump during positive IOD while increase in pCO_2 due to the increase in carbonate pumps. The net effect is the summation of all. (right) It is found that the pCO_2 increase due to the carbon enrichment in the surface overwhelms all other impacts and leads southeastern tropical Indian to a source of CO_2 during positive IOD.

The ocean plays a vital role in mitigating global climate change by sequestering ~30% of anthropogenically emitted carbondioxide (CO_2) per year (Sabine et al., 2004; Valsala and Maksyutov, 2010; Le Quéré et al., 2018; Friedlingstein et al., 2019; Gruber et al., 2019). In the absence of this sink, the accumulation of human-made CO_2 in the atmosphere could have been amplified by a corresponding magnitude, and global warming would have been much more accelerated. The global ocean has taken up nearly 165 ± 20 petagrams of carbon (PgC) emitted since the pre-industrial era (Le Quéré et al., 2018). The contemporary global ocean CO_2 sink is estimated to be 2.5 ± 0.6 peta gram carbon per year (Pg C yr^{-1}; Friedlingstein et al., 2019).

Tropical Indian Ocean (IO) alone contributed to sinking 17.2 ± 5.6 petagrams anthropogenic carbon, amounting a 16% of the global total ocean sink (Olsen et al., 2020). The recent synthesis of the Indian Ocean (north of 40°S) sea-to-air CO_2 flux suggests an annual mean (median) CO_2 uptake of -0.37 ± 0.06 Pg C yr^{-1} based on models and a sink of -0.24 ± 0.12 PgC yr^{-1} based on observational estimates, for a period of 1990-2010 (Table-3, Sarma et al., 2013).

The most popular interannual variability in the tropical Indian Ocean is known as Indian Ocean Dipole (IOD) Mode. It significantly influences Asian and Australian Monsoon systems and tele-connected to other major tropical-to-mid latitude oceans. However, the role of IOD in Indian Ocean carbon cycle variability was poorly known. Using 60 ye ars of model simulations and available observations, we examined the relation between IOD and carbon cycle variability in the upper oceans of the southeastern tropical Indian Ocean. The results show that a positive (negative) IOD causes positive (negative) anomalies of sea-to-air CO_2 fluxes, surface ocean pCO_2, concentrations of surface ocean dissolved inorganic carbon, and surface ocean alkalinity. The dissolved inorganic carbon and alkalinity dynamics, together with freshwater forcing, control the southeastern tropical Indian Ocean's carbon cycle variability due to IOD. The study also identifies the similarities and differences of southeastern tropical Indian Ocean compared to the eastern tropical Pacific.

References:

Friedlingstein, P., Jones, M. W., O'Sullivan, et al.,(2019), Global Carbon Budget 2019, Earth Syst. Sci. Data, 11, 1783–1838

Gruber, N., D. Clement, B. R. Carter, R.A. Feely, et al., (2019), The oceanic sink for anthropogenic CO_2 from 1994 to 2007, Science, Vol. 363, Issue 6432, pp. 1193-1199.

Le Quéré, C., Andrew, R. M., Friedlingstein, P., et al., (2018), Global Carbon Budget 2018, Earth Syst. Sci. Data, 10, 2141–2194

Olsen, A., Lange, N., Key, R. et al., (2020), GLODAPv2.2020 – the second update of GLODAPv2. . doi:10.5194/essd-2020-165

Sabine, C. L., Feely, R. A., Gruber, N., et al., (2004), The oceanic sink for anthropogenic CO_2 , *Science,* 305, 367 – 371, doi:10.1126/science.1097403.

Saji, N., Goswami, B., Vinayachandran, P. *et al* (1999), A dipole mode in the tropical Indian Ocean. *Nature* **401,** 360–363

Sarma, V. V. S. S., Lenton, A., Law, R. M., Metzl, N., Patra, P. K., Doney, S., Lima, I. D., Dlugokencky, E., Ramonet, M., and Valsala, V. (2013), Sea–air CO_2 fluxes in the Indian Ocean between 1990 and 2009, *Biogeosciences,* 10, 7035-7052

Valsala, V., and Maksyutov, S. (2010), Simulation and assimilation of global ocean pCO_2 and sea-to-air CO_2 fluxes using ship observations of surface ocean pCO_2 in a simplified biogeochemical offline model. *Tellus-B Vol.* 62: 821-840.

Activities of Ocean Society of India (OSI) during 2018-2020

Kerala deluge and 2018 monsoon

The Ocean Society of India – Kochi Chapter in the wake of the very active southwest monsoon and resulting unusual flood in Kerala organized a 'Panel Discussion' in Kochi jointly with Centre for Marine Living Resource and Ecology (CMLRI-MoES) and National Institute of Oceanography (CSIR-NIO, RC Kochi) on 5th October 2018. Ockhi cyclone 2017 and Kerala flood August 2018 were two major discussion topics. An expert panel discussed the various aspects in the Panel Discussion with a major objective to analyse scientifically the causative factors for the 2018 monsoon and its impacts in Kerala and came up with a few recommendations for future action. Altogether about 50 participants from various institutes from India attended and actively involved in the deliberations and discussion. The recommendations emerged out of the day long discussions were submitted to the various agencies for further action.

World Oceans Day

Ocean Society of India (OSI) observed the world oceans day on 8th June 2019 at Mararikkulam Beach. The programmes conducted were: Interactive Sessions on various aspects of oceans and beach cleaning. The interactive awareness programme on oceans was conducted in which 90 students from High School to College level, Active fishermen who are deeply involved in ocean conservation, teachers, officials from CMLRE, NIO, NPOL, Universities, NGOs participated

Ocean Science Outreach

The Ocean Society of India conducted awareness programme at Sree Narayana College, Cherthala on 12/01/2018 for school children as part of its outreach programme. The function started with an inauguration followed by three talks: Prof. Dr. K. S. Purushan, Former Dean Fisheries, KAU, gave a talk on Oceans, its importance in economy, food security, climate; Dr. C V K Prasada Rao, Former Chief Scientist of NPOL delivered a talk on climate, weather, calamities in ocean, tsunami, Ockhi cyclone and ocean currents; Dr. Dhanya Viswam, Assistant Professor, S N College delivered a talk on chemistry of sea water.

Ocean Modeling Workshop for Students and Research Scholars (OSIMOD 19)

OSI and Kerala University of Fisheries and Ocean Studies (KUFOS) jointly organised a workshop on Ocean Modeling for Students and Research Scholars (OSIMOD 19) at KUFOS, Panangad, Kochi during 11-14 June 2019. The sole objective of it is to provide hands-on experience with two important contemporary ocean models, namely, Simulating Waves Nearshore (SWAN) and Regional Ocean Modeling System (ROMS; ocean circulation model) which are used for operational ocean forecasting purposes at many places over the globe. Prof. Prasad K Bhaskaran and Prof. Arun Chakraborthy, both from IIT, Kharagpur have demonstrated the above two models to the participants of OSIMOD 19.

National Seminar on Climate Change and Coastal Ocean Processes (CCCOP-2019)

The Ocean Society of India (OSI) organized a National Seminar on "Climate Change and Coastal Ocean Processes" (CCCOP-2019) at Centre for Atmospheric Sciences, Indian Institute of Technology Delhi during 4-5 July 2019. The Seminar was co-sponsored by India Meteorological Department, Government of India. It was a great success in fulfilling its aims with the contributions from eminent scientists, researchers and students from a wide range of institutes across the country. There was a total of 13 lead talks and 30 presentations in the seminar.

OSICON-2019

OSI organized its 6th Biennial conference (OSICON-19) at the Centre for Marine Living Resources & Ecology (CMLRE), Kochi, Kerala, during12-14 December 2019. Around 130 oral presentations and 65 poster presentations from various researchers including invited and lead talks from the experts are the main highlights of OSICON-19.

OSI Awards and Honours-Dr Devanatha Srinivasan Endowment Award and PG-Dissertation Awards

OSI has instituted an award in the name of Dr. D. Srinivasan, former Director of NPOL. The award is to be given once in two years commencing from the year 2019. The first award was shared by two leading researchers namely: Dr. Muthalagu Ravichandran, Director, NCPOR, Goa and Dr. Bishwajith Chakraborty of NIO, Goa. The OSI Cochin Chapter announced awards to meritorious PG students for the academic year 2018-19 based on their dissertations.

OSI Webinar Series

In view of the global pandemic COVID-19 and the social distancing norms, OSI could not take up new outreach activities like flagship training programme OSIMOD, World Oceans Day observation and associated awareness progrmmes during 2020. Therefore in the GC meeting held in 20 June 2020, it was decided to organize online webinar lecture series of one hour duration. OSI conduct 3 webinars through Google Meet and was well appreciated by the Ocean community across the country.

Call for contributions

Articles/research highlights of general interest to the oceanographic community are invited for the next issue of the Ocean Digest. Contributions may be emailed to **osioceandigest@gmail.com**